Observing Conditions at Mt. Graham: VATT $UBVR$ Sky Surface Brightness and Seeing Measurements from 1999 through 2003.

Violet A. Taylor

violet.taylor@asu.edu

Rolf A. Jansen

rolf.jansen@asu.edu

and

Rogier A. Windhorst

rogier.windhorst@asu.edu

Department of Physics and Astronomy, Arizona State University, Box 871504, Tempe, AZ 85287-1504

ABSTRACT

We present measurements of sky surface brightness and seeing on Mt. Graham obtained at the Vatican Advanced Technology Telescope (VATT) during 16 observing runs between April 1999 and December 2003. We show that the sky surface brightness is significantly darker during photometric conditions, and can be highly variable over the course of a single observing run as well as from one run to the next, regardless of photometricity. In our photometric observations we find an average low-airmass ($\sec z < 1.2$) sky surface brightness of 22.00, 22.53, 21.49, and 20.88 mag arcsec^{-2} in U, B, V, and R, respectively. The darkest run (02/00 in U and 02/01 in BVR) had an average sky surface brightness of 22.38, 22.86, 21.72, and 21.19 mag arcsec^{-2} in U, B, V, and R, respectively. With these results we show that under the best conditions, Mt. Graham can compete with the darkest sites in Hawaii and Chile, thanks in part to the strict dark-sky ordinances in place in Tucson and Safford. We expect the sky over Mt. Graham to be even darker than our 1999–2003 results during solar minimum (2006–2007).

We find a significant improvement of about $0.45''$ in our measured stellar FWHM after improvements to the telescope were made in Summer and Fall 2001. Stellar FWHM values are highly variable, with median R-band focus FWHM values in each observing run ranging from $0.97''$ to $2.15''$. Significantly subarcsecond seeing was occasionally achieved with values as low as $0.65''$ FWHM in

R. There may possibly still be a significant telescope contribution to the seeing at the VATT, but nearby trees as high as the dome are currently the dominant factor.

Subject headings: atmospheric effects – light pollution – site testing – telescopes

1. Introduction

Mount Graham International Observatory (MGIO) is located near Safford, Arizona at an altitude of 10,400 feet. It contains the Vatican Advanced Technology Telescope (VATT), the Heinrich Hertz Submillimeter Telescope, and the Large Binocular Telescope[1] (LBT; currently under construction with first light expected in late 2004). The observing conditions at the MGIO site are important limiting factors on the efficiency of observing faint objects, and are thus important to characterize with observations at the existing telescopes, as well as the LBT. Therefore, in this paper we focus on two of the most important properties of an observing site: the sky surface brightness and the seeing over the course of four years.

Dark sites are in increasingly short supply due to metropolitan development, but reasonably dark sites do still exist. Other observers have studied sky surface brightness values at other observing sites, particularly in the context of determining the effects of nearby city lights. Massey and Foltz (2000) measured the sky brightness in various directions of the sky at Kitt Peak and Mt. Hopkins in 1988 and again in 1998 to determine the effects of increasing light pollution from the expansion of Tucson. They found that since 1988, the zenith BV sky brightness increased slightly by 0.1–0.2 mag arcsec^{-2} at Kitt Peak. At a larger zenith distance of 60°, however, there was a 0.35 mag arcsec^{-2} increase when pointing away from Tucson, and a 0.5 mag arcsec^{-2} increase when pointing toward Tucson. They mention that this increase in sky brightness would be worse if Tucson did not have good outdoor lighting ordinances, which also exist in Safford. Although Mt. Graham is near Safford, Safford is a much smaller city than Tucson and MGIO is located at a much higher elevation than Kitt Peak and Mt. Hopkins, with Tucson and Phoenix well below the horizon as viewed from the Mt. Graham summit. Hence, city lights should not have as large of an impact on the sky brightness at MGIO.

Other factors in addition to city lights impact the sky brightness, such as the presence of atmospheric dust, forest-fire smoke, cirrus, the solar cycle, airmass, galactic and ecliptic latitude of the observation, the phase and angular distance of the Moon from the observed

[1]http://medusa.as.arizona.edu/lbto/

object, and altitude and geomagnetic latitude of the observing site. Benn and Ellison (1998) measured the sky brightness at La Palma from 1987 to 1996, finding that the sky was 0.4 mag arcsec^{-2} brighter during solar maximum than solar minimum, and 0.25 mag arcsec^{-2} brighter at an airmass ($\sec z$) of 1.5 than an airmass of 1.0 (at the zenith). Krisciunas (1997) measured the sky brightness at Mauna Kea in Hawaii, and found that except for the solar cycle, the most important effect is random short term variations over tens of minutes, which makes sky brightness measurements highly variable and difficult to compare between sites. To quantify the quality of sky brightness at Mt. Graham, we present our sky surface brightness measurements from April 1999 to April 2002 at the VATT, compare our measurements to those known at Mt. Hopkins, Kitt Peak, Mauna Kea, La Palma, ESO, and Cerro Tololo, and discuss how the variability of sky brightness due to the factors listed above impact our conclusions. We also compare our measurements to a theoretical sky brightness for Mt. Graham (Garstang 1989) and investigate the effects of city lights and the variation of sky brightness with time of night.

The seeing of an astronomical site can be estimated by measuring the median full width at half max (FWHM) of stars in images taken at that site. We have done this for Mt. Graham by measuring the FWHM of stars in stacked galaxy images and in short focus exposures taken at the VATT. This is only an estimate, because there are other factors in addition to atmospheric seeing that play a role in the stellar FWHM, such as telescope focus and telescope image quality due to mirror quality, telescope collimation, etc.. The FWHM results presented in this paper are to be applied at face value to the VATT alone, and do not necessarily reflect on the Mt. Graham site or on the LBT site, since the VATT's specific location on the mountain-top makes it more susceptible to ground layer seeing, particularly in northeasterly winds.

2. Observations

We have obtained $UBVR$ surface photometry for 142 galaxies at the VATT, using the VATT 2k×2k Direct CCD Imager. Typical exposure times were 2×(600–1200)s in U, 2×(300–600)s in B, 2×(240–480)s in V, and 2×(180–360)s in R. The CCD gain is 1.9 electrons per ADU and the read-noise is 5.7 electrons. We binned the images 2×2, resulting in a pixel scale of 0.375 arcsec pixel^{-1}. Individual images were stacked with integer shifts, as the PSF is well sampled. Sky brightness values and FWHM values measured from stacked images are the signal-to-noise weighted average values from the individual images that make up the stack, which suffices to examine overall trends in the data. The details of our galaxy sample and galaxy surface photometry, and the methods we used for data reduction and

calibration are presented in a separate data paper on our nearby galaxy survey (V. Taylor, et al., in preparation).

Observations were spread over 9 runs between April 1999 and April 2002, for a total of 49 usable nights. Defining photometric nights as those with zeropoint magnitudes that vary no more than 3% throughout, 45% of the nights were photometric, 51% were mostly non-photometric (with parts of the night possibly photometric until clouds moved in), and 4% were lost entirely to telescope problems. During nights where clouds appeared toward the end of the night, we salvaged as much as possible of the first part of the night as photometric.

For comparison, additional focus exposure stellar FWHM values are presented for 8 VATT observing runs between November 2001 and December 2003, which were carried out independently by R.A. Jansen for other projects.

3. Trends in Sky Surface Brightness at the VATT

3.1. Measurements of the Sky

Sky values for each stacked galaxy image were calculated by finding the median of the median pixel value in each of 13 boxes, each 120 pixels wide, along the edges of the image. This was done to avoid including light from the galaxy, which was usually centered in the CCD. Taking the median values helps to reject stars and cosmic rays, which comprise a small percentage of the total number of pixels in the sky boxes. The average sky count-rates for all stacked galaxy images were 0.41 ± 0.01 ADU s^{-1} in U, 1.34 ± 0.11 ADU s^{-1} in B, 2.64 ± 0.10 ADU s^{-1} in V, and 4.26 ± 0.15 ADU s^{-1} in R. Sky surface brightness values were photometrically calibrated using Landolt standards (Landolt 1992). We defined photometric nights as those with zeropoints that vary no more than 3% throughout the night, which defines the largest uncertainty in the calibrations.

3.2. Sky Surface Brightness Results

In Figure 1, the resulting $UBVR$ sky surface brightness values for each stacked galaxy image are plotted vs. the average airmass ($\sec z$) of the individual images that comprise each stack. Each observing run is broken up into a separate panel for comparison. Stacked images that are comprised solely of individual images taken during photometric conditions (change in magnitude zeropoint throughout the night $\lesssim 3\%$) are plotted as asterisks, while those comprised of images taken during non-photometric conditions are plotted as open circles.

There is a clear, well defined difference in sky surface brightness between these two conditions: non-photometric nights have notably brighter skies, as expected due to the presence of cirrus. There is a trend of increasing sky surface brightness with increasing airmass, which is also to be expected, although there does not appear to be a single consistent slope to this trend throughout all observing runs, even for photometric runs. It is also apparent from the plots in Figure 1 that the sky surface brightness is highly variable as a function of time, both over the course of a single run and from one run to the next. Since the sky brightness is highly dependent on many factors, such as solar activity, atmospheric conditions, time since sunset, variable night sky-lines, and the location of the telescope pointing with respect to nearby city lights, the Moon, zodiacal light, and the Galaxy itself, this variability is not surprising.

The effect of the Moon on the sky surface brightness of a given galaxy field is a complicated function of the phase of the Moon, the airmass ($\sec z$) of both the Moon and the galaxy position, the angular distance between the Moon and the galaxy (θ_{Mg}), and the atmospheric extinction (Krisciunas & Schaefer 1991). We approximate the effect of Moon on our sky surface brightness (μ) results through a plot of the sky brightness of all stacked galaxy images vs. $\cos\theta_{Mg}$, which is shown in Figure 2. We use $\cos\theta_{Mg}$ because the effects from the Moon on the sky brightness of a target away from the Moon may behave as a spherical harmonic, so that some linear behavior in $\cos\theta_{Mg}$ may be expected. The secondary Moon effects due to airmass of the Moon and galaxy and atmospheric extinction are not separated out here, and are expected to be small compared to other large scale variations in the overall sky surface brightness, as discussed previously. The sky brightness values were normalized to the median sky brightness for the relevant observing run in order to remove large-scale seasonal effects. Four sub-panels show different Moon phases, ranging from a Moon illumination of 0% to 40%, which is the maximum illumination in our data. This plot shows that photometric nights (indicated by solid symbols) tend to have darker skies than non-photometric nights (open symbols), and show a smaller scatter in sky surface brightness from one image to the next. Both photometric and non-photometric exposures show no major trend with Moon angular distance within the scatter for Moon illumination $\leq 20\%$. There may be a slight anti-trend of increasing sky surface brightness at 180° from the Moon visible in the panel for Moon illumination $\leq 10\%$, which could be the result of sun-light back-scattering off of the atmosphere. A stronger trend of increasing sky surface brightness with decreasing Moon angular distance is apparent when Moon illumination is $\geq 20\%$. We applied a linear least-squares fit of

$$\mu = m\ \cos\theta_{Mg} + b \tag{1}$$

to this trend for the mostly photometric data in the Moon illumination $\geq 30\%$ panel (eliminating points with airmass > 2), and determined slopes of 0.97 in U, 0.83 in B, 0.36 in V, and 0.29 in R. Thus, as expected, there is a stronger dependence on Moon angular distance

for shorter wavelengths. There are only a small number (∼5) of galaxy images that are affected by the Moon within the scatter of these plots, leading us to the conclusion that our median sky surface brightness values are largely unaffected by moonlight.

Solar maximum occurred around 2000–2001, in the middle of the time spanned by our observations, which could have raised the sky surface brightness by several tenths of a magnitude with respect to the sky surface brightness at solar minimum. For instance, Benn and Ellison (1998) saw an increase in sky brightness of 0.4 magnitudes in $UBVR$ from solar minimum to solar maximum at La Palma. We therefore expect the sky surface brightness to be fainter than these results by a similar amount during the upcoming solar minimum (2006–2007).

The dotted lines in Figure 1 (B and V panels) represent an estimate of the dependence of the sky surface brightness on airmass at Kitt Peak and Mt. Hopkins as measured by Massey and Foltz (2000) for comparison. Zenith values (airmass=1.00) were derived by taking the average of Massey and Foltz's measurements at both locations, which consisted of 1 exposure in each passband at Mt. Hopkins in Nov. 1998, and 4 exposures in each passband at Kitt Peak over three nights in Nov. 1999 (all of which were just before solar maximum, like our earlier runs. However, our later runs are closer to the solar maximum peak, and thus will be brighter). We calculated an average high airmass sky surface brightness by taking the average of 4 exposures in each passband at Mt. Hopkins at zenith distances of $34 - 53°$, and 6 exposures in each passband at Kitt Peak at zenith distances of ∼60°. The dotted lines in Figure 1 connect these two points, assuming a linear dependence on airmass, which is roughly correct. One should be cautious when comparing sky brightness measurements for different sites, due to the strong variability over time visible in these figures, especially in a case like Mt. Hopkins/Kitt Peak, where we have no information on long-term variations. An additional source of uncertainty arises because Massey and Foltz (2000) derived their broadband sky brightness values from spectrophotometry, replacing the variable O I λ5577 line with an average value. Nonetheless, we can see that several VATT observing runs had sky surface brightness values that were significantly darker than the Mt. Hopkins/Kitt Peak numbers given by Massey and Foltz (2000), who point out that their numbers are comparable to Palomer Observatory in the early 1970's, which was considered a rather dark site at the time.

Figure 3 shows the median sky surface brightness at the VATT, per observing run, of all low airmass ($\sec z < 1.2$) stacked galaxy images taken during photometric conditions, as a function of time. One obvious outlying sky brightness value was rejected in the 1/02 run in U and B, which was measured near morning twilight, and therefore contaminated our results. For comparison, we overlay the average values from Mt. Hopkins/Kitt Peak,

(Massey & Foltz 2000), Cerro Tololo, (Walker 1987, and 1987–1988[2]), and La Palma, (Benn & Ellison 1998). Again, we caution against putting strong confidence in such comparisons for the reasons previously mentioned. On occasion the VATT was darker than Cerro Tololo, except in the V-band. The La Palma observations were taken from 1987 to 1996, and the values plotted in Figure 3 are the solar minimum values given by Benn and Ellison (1998) minus the quoted 0.4 magnitude difference between solar minimum and maximum, since our data was taken near solar maximum. For the most part, our values are consistently darker than La Palma's solar maximum skies, and similar to La Palma solar minimum skies (sometimes brighter, sometimes darker, although always brighter in the V-band). Figure 3 clearly shows a strong variability of several tenths of a magnitude in sky brightness from observing run to observing run, with a general brightening of the sky toward solar maximum (2000–2002). The anomalously bright point during solar minimum in 1999 may have been due to smoke from nearby forest fires.

In Table 1 we list our average photometric low airmass sky surface brightness values for the VATT, Mt. Graham, and for various other sites for comparison. We also give sky surface brightness values for our darkest and brightest runs. Excluding the Mauna Kea solar maximum values (Krisciunas 1997), which are significantly brighter than any of the measurements for the other sites, the darkest B-band sky surface brightness at sites other than Mt. Graham range from 22.6 to 22.84 mag arcsec^{-2}, compared to our average value of 22.53 mag arcsec^{-2}. Our darkest run was 22.86 mag arcsec^{-2}, which is marginally darker by 0.02 mag arcsec^{-2} than the darkest site (Mauna Kea at solar minimum). Since our observations were made near solar maximum, we can expect the Mt. Graham site to become darker still during periods of low solar activity in 2006–2007. Sites other than Mt. Graham had V-band sky brightness values that varied between 21.44 and 22.29 mag arcsec^{-2}, compared to the Mt. Graham average of 21.49 mag arcsec^{-2}. Our darkest run had a V-band sky surface brightness of 21.72 mag arcsec^{-2}, which is 0.28 mag arcsec^{-2} darker than the brightest site (Kitt Peak (Massey & Foltz 2000)) and 0.48 mag arcsec^{-2} brighter than the darkest site (CTIO during solar minimum (Phillips 1997[3])), although, again, our observations were at solar maximum. There are fewer published sky surface brightness values in U and R, but where we can make a comparison (La Palma (Benn & Ellison 1998), ESO (Patat 2003), and Cerro Tololo (Walker 1987)), our Mt. Graham averages are similar, and our darkest run was 0.08 mag arcsec^{-2} darker in U than ESO and 0.19 mag arcsec^{-2} darker in R than La Palma.

We can compare our measured sky brightness values to the Garstang (1989) predicted

[2]http://www.ctio.noao.edu/site/pachon_sky/

[3]http://www.ctio.noao.edu/site/pachon_sky/

V- and B-band sky surface brightness values for Mt. Graham. Garstang calculated V-band sky brightness values for very clear air, during solar minimum, and using 1980 populations for nearby towns and cities. This resulted in a predicted V-band sky brightness of 21.94 mag arcsec^{-2} for MGIO at the zenith, and 21.72 mag arcsec^{-2} at a zenith distance (z) of 45°. This agrees well with our darkest run which had an average V-band sky surface brightness of 21.72 ± 0.04 mag arcsec^{-2} for z $\lesssim$ 33.6°. Our measured value is slightly brighter than what would be expected from Garstang's predictions, but this can easily be explained by an increase in population since 1980 and the fact that our measurements were taken near solar maximum. Garstang also predicted B-band sky surface brightness values of 22.93 mag arcsec^{-2} at z=0° and 22.75 mag arcsec^{-2} at z=45°, which agrees well with our darkest run, with an average B-band sky surface brightness of 22.86 mag arcsec^{-2} for z $\lesssim$ 33.6°.

To determine how nearby city lights affect sky brightness, we plot sky surface brightness vs. the azimuth (az) of our observations in Figure 4. Data taken during nights where Moon illumination $\geq$ 20% were rejected from this plot. We normalized the sky brightness of each image to the median sky surface brightness for the sec $z \leq 1.3$ data in each observing run, and arbitrarily offset data-points taken during non-photometric conditions from those taken during photometric nights. Open circles (non-photometric) and solid circles (photometric) represent images taken at mid-zenith distances ($20° \leq z < 40°$), while asterisks (non-photometric) and triangles (photometric) represent images taken at high-zenith distances ($z \geq 40°$). Vertical dotted lines mark the general direction of three cities that may contribute to light-pollution at the Mt. Graham site.

Figure 4 shows that images observed toward the North during photometric conditions tend to have darker skies than all other directions. Darker northern skies are seen to a lesser extent with increasing wavelength (0.2, 0.1, 0.06, and 0.00 mag arcsec^{-2} darker than the median sky in U, B, V, and R, respectively), and not at all in the non-photometric data (due to the presence of cirrus). This implies that the effect may be due more to the large angular distance of these pointings from the zodiacal belt and Milky Way than to the absence of city lights in that direction. Phoenix and Tucson contribute somewhat to the sky brightness, with photometric skies between the two cities ($220° < az < 300°$) brighter than the median sky by 0.1 mag arcsec^{-2} in U, and 0.2 mag arcsec^{-2} in BVR. This brightening toward Tucson and Phoenix is strongest at high zenith distances ($z \geq 40°$) and during non-photometric conditions, which is consistent with the expected reflection of city lights off of clouds or cirrus. Safford has less of an effect on sky brightness, however, with no measurable brightening in that direction during photometric conditions. The only exception is in the R-band during non-photometric conditions, where the sky in that direction is 0.4 mag arcsec^{-2} brighter than the median. This might be at least in part due to sodium lamps from Safford, which emit at 5500–6500 Å, and are therefore most apparent in R ($\lambda_e \sim 6340$ Å). This is

consistent with Massey & Foltz (2000), who estimated the contribution of such lamps in Tucson to be 0.17 mag arcsec^{-2} at the zenith of Kitt Peak and Mt. Hopkins, with a larger effect expected at higher zenith-distances and with the presence of clouds. Our brightest sky measurements toward Safford are outlying non-photometric, high-airmass data-points, and overall Safford contributes very little to the night sky brightness at the location of the VATT on Mt. Graham. Garstang (1989) predicted that the night sky would be brightest toward Safford at a modest zenith distance of 45°, and considerably brighter toward Tucson than any other direction at the extreme zenith distance of 85°. However, Tucson affects our sky brightness measurements more than Safford in almost all cases. This is in part because the Safford lights are shielded by the mountain peak at the VATT's location, and in part because of the strict dark-sky ordinances in place in Safford, as well as faster growth in Tucson than Safford since Garstang's 1980 population calculations. Also, smog carried up from the Tucson valley to the nightly inversion layer likely reflects the city lights better than the clean air above Safford. Overall, city lights have little affect on the sky brightness at Mt. Graham, making it a prime dark-sky site.

Sky brightness can also vary with time of night, as addressed by Walker (1988). Walker found an exponential decrease in sky brightness at San Benito Mountain of 0.4 mag in B and V during the first half of the night. Since this decrease was observed near the zenith, and was independent of overall sky brightness, time of year, and the presence of fog, Walker concluded that it is more likely due to a natural phenomenon than a decrease in the contribution of city lights throughout the night. Walker mentions that this may be partially due to a decrease in the zodiacal light contribution throughout the night, but is likely mostly due to the recombination of ions that were excited during the day by solar EUV radiation.

We investigate this trend at Mt. Graham in Figure 5, which shows the dependence of sky surface brightness in $UBVR$ on fraction of the night, where the beginning and end of the night in each run is defined as the end and beginning of astronomical twilight for the mid-point of that run. We plot only data-points taken during moon illumination $\leq 20\%$ and at z $\leq 40°$. We normalized the sky brightness of each image to the median sky surface brightness for the $\sec z \leq 1.3$ data in each observing run, and arbitrarily offset data-points taken during non-photometric conditions from those taken during photometric nights by 1.5 mag. We approximate the nightly sky brightness trend with a linear least-squares fit that does not include measurements taken within 0.5 hours of twilight (solid lines). The UB photometric data show no significant trend with time of night. There is, however, a trend in photometric data in V and R (which is expected due to the nightly decrease in O I λ5577 and λ6300-34 emission line strengths), with a decrease in the first half of the night of 0.1 mag arcsec^{-2} in V and 0.2 mag arcsec^{-2} in R, followed by a slight increase in sky brightness toward the very end of the night. This is less than the 0.4 mag arcsec^{-2} decrease seen in B

and V by Walker (1988), which may be due to the difference in elevation of Mt. Graham (10,400 feet) and San Benito Mountain (5248 feet). This highlights one of the advantages of Mt. Graham's high elevation, which contributes in many ways to making it a particularly dark site. Non-photometric data shows a stronger trend, with an overall decrease in sky brightness throughout the night of 0.2, 0.3, 0.3, and 0.4 mag arcsec^{-2} in U, B, V, and R, respectively. The reason for this decrease in sky brightness is uncertain at this time, but may be related to a general decrease of cloud-cover throughout the night, which we often recorded in the observing logs. Local humidity-driven weather induced by Mt. Graham itself may be responsible for this, especially in late spring–early fall, when the humidity is higher.

4. Trends in Estimated Seeing, or Stellar FWHM at the VATT

4.1. Measuring the Stellar FWHM

The FWHM of stars measured with the VATT 2kCCD is affected by the telescope focus in addition to atmospheric effects. The actual focus value depends on several factors, such as optics, temperature, airmass, and filter. Since the VATT has a fast $\sim$ f/1 primary mirror, its focus is very sensitive to changes in temperature during the night. Once the telescope has reached equilibrium with the night air, the automated telescope software adjusts the focus to account for temperature and airmass changes. Particularly at the start of each night, however, it is necessary for the observer to frequently refocus the telescope as the temperature drops. Also, as the focus changes throughout the night the FWHM may deteriorate progressively over time, which raises the average stellar FWHM values with respect to the actual atmospheric seeing. Consistently rechecking the focus throughout the night can minimize this effect. Since these data were taken as part of a galaxy survey that focuses mainly on U-band galaxy surface photometry, we typically only focused in U. The change in focus between filters is small, since all of the filters are nearly par-focal, but focusing only in U may have resulted in a slightly larger average seeing value in B, V, and R than could have been obtained if the images had been focused in each filter separately. Therefore, we offer a cautionary note that the FWHM values in our galaxy images are likely larger than what we could achieve at the VATT if they each had been focused in their particular target filter, and if each galaxy image had been preceded by a focus check. Also, since the FWHM's from the galaxy images presented in this paper were measured from stacked images, they will be marginally larger than if we measured them from the individual images. This is due to small errors in image alignment from the applied integer shifts.

We measured the stellar FWHM for all of our stacked galaxy images with the LMORPHO package (Odewahn, et al. 2002), which imports a list of all sources and their FWHM's

produced with SExtractor (Bertin & Arnouts 1996). Stars are selected from the source list for each image by interactively defining limits on a plot of FWHM vs. magnitude, like the one shown in Figure 6. As can be seen on this plot, the FWHM of stars does not significantly depend on their brightness (except for bright saturated stars), while brighter galaxies tend to be larger in size, creating a quick way of identifying stars. This semi-automated method works well for most galaxy images, although problems may occur for fields that contain very few bright stars. In such cases, our seeing estimate may be too large, since the star selection may be contaminated by some faint extended objects.

To obtain more accurate measurements of the atmospheric seeing than can be measured with the galaxy images, we also measure the FWHM of the stars with the best focus in our focus exposures using `IMEXAM` within IRAF.[4] These focus exposures are single images in which 5-7 short exposures at different focus settings are recorded, where prior to each exposure the charge on the CCD is shifted by 50-100 pixels. Because these exposures are short, the stellar images are not affected by tracking and guiding errors or by telescope vibrations (as we will show below, this was particularly a problem in our earlier runs). Independent FWHM measurements by two of us (Taylor and Jansen) agree to within the measurement errors (typically $\sim$0.05–0.10$''$).

4.2. Estimated Seeing Results

Figure 7 shows the median FWHM of stars measured in our stacked galaxy images as a function of airmass in $UBVR$, and is split into separate panels for each observing run. There is a clear trend of increasing FWHM with airmass, which is to be expected from the theoretical relation[5] of

$$\mathrm{FWHM}(z) = \mathrm{FWHM}(0)\, sec(z)^{0.6} \tag{2}$$

but, like the sky surface brightness, this trend does not seem to have a particularly consistent slope from one run to the next (possibly because the automatic focus did not correct for airmass dependence accurately enough). Stacked images that are comprised solely of individual images taken during photometric conditions (variation in magnitude zeropoint throughout the night $\lesssim 3\%$) are plotted as asterisks, while those comprised of images taken during non-photometric conditions are plotted as open circles. This reveals that there does

[4]IRAF is distributed by the National Optical Astronomy Observatories, which are operated by the Association of Universities for Research in Astronomy, Inc., under cooperative agreement with the National Science Foundation.

[5]http://www.ing.iac.es/Astronomy/development/hap/dimm.html

not seem to be a clear trend of seeing with photometricity. However, we note that in the two runs (April 1999 and May 2000) where there is a significant difference between the seeing in the photometric nights and in the non-photometric nights, the non-photometric nights had better seeing. The observation log sheets noted the presence of cirrus, which is often correlated with stable air and better seeing. Solid squares in this plot represent the FWHM of the stars with the best focus in the short focus exposures. These FWHM values tend to be smaller than or equal to the stellar FWHM measured in galaxy images taken immediately after the focus exposures, for the reasons mentioned in the previous section. As the telescope focus degrades with time between focus exposures, the stellar FWHM in the galaxy images will increase. Thus, the focus FWHM values are indeed a more accurate measurement of the atmospheric seeing.

Figure 8 shows the median low airmass ($\sec z < 1.2$) FWHM values for each run, with solid circles representing the stellar FWHM in the stacked galaxy images, and open circles representing the best focus FWHM in the focus exposures. In almost all cases, the median FWHM in the focus exposures is smaller than that in the galaxy images, as expected. Except for the February 2001 observing run, which had particularly good seeing, it is apparent that the average FWHM values and their uncertainties (which reflect the range of the data) are much larger for the runs before May 2001. This change in FWHM values corresponds to an engineering run at the telescope in Summer 2001, during which time a vibration in the secondary mirror mount that had contributed up to $0.4''$ to the FWHM was removed (M. Nelson, private communication). Adjustments were also made to the pointing map in Fall 2001. As Figure 8 shows, both of these improvements resulted in a significant reduction of the FWHM of the VATT PSF. Table 2 lists the average of the median stellar FWHM values in the galaxy images for all runs (ignoring the outlying April 2001 run) before and after the improvements. There was an overall improved seeing of about $0.45''$ in all filters, as well as a more stable focus, as can be seen in the decreased FWHM scatter between these two time periods in Figure 7, and the smaller uncertainties in Figure 8 and Table 2. After the improvements, we were able to obtain sub-arcsecond seeing in one of our combined images in R in April 2002 (see Figure 7), even though we focused in a different filter, and routinely measured sub-arcsecond seeing in the focus frames.

The stellar FWHM values from the galaxy images are useful in determining the average FWHM that one might realistically achieve in long (3–20 minute) object exposures at the VATT, with better results possible with more frequent focusing, and with refocusing done for each filter. However, the best FWHM values are obtained through the shorter (several second) focus exposures.

We can inter-compare the FWHM in focus exposures taken in different filters by de-

termining the offset in the PSF between filters, which is a result of both the wavelength dependence of atmospheric seeing and the contribution of the telescope. Atmospheric seeing has been studied extensively in the past (e.g. Kolmogorov 1941, Tatarski 1961, and Fried 1965), and has been reviewed and summarized more recently by Coulman (1985) and Roddier (1981). The *Fried parameter*, r_0, is a measure of the average effective size at a given wavelength, λ, of the elements of air that are responsible for the angular deviations of light from a distant point source, which is the cause of atmospheric seeing. Where $r_0 \propto \lambda^{6/5}$, the FWHM measured in seeing estimates is related to r_0 by

$$\mathrm{FWHM} = 0.98\,\lambda\,r_0^{-1} \tag{3}$$

which results in a dependence of the FWHM on wavelength of $\lambda^{-1/5}$. To test this relation and find the FWHM contribution from the telescope, we plot the stellar FWHM of our images in each filter minus the stellar FWHM for that field in the R band (Figure 9). We only include galaxies where exposures in each filter were taken immediately after one another in order to limit the effects of airmass and large-scale seeing changes between exposures during the night. The outlying points were likely due to fields imaged during highly variable seeing conditions, or to fields where a focus exposure was taken in between observations. The solid curve in Figure 9 traces the theoretical $\lambda^{-1/5}$ FWHM dependence, while the crosses mark the median FWHM_λ – FWHM_R offset from the $\lambda^{-1/5}$ relation. The slight offset between the observational medians and the theoretical $\lambda^{-1/5}$ line gives the systematic contribution of the telescope to the wavelength dependence of the stellar FWHM. The scatter in this plot gives a measure of the random contribution of the atmosphere and telescope to the wavelength dependence, which can be due both to atmospheric variations and telescope vibrations (which is more important for the earlier runs, before the telescope improvements made in Summer and Fall 2001). These factors cannot be separated from one another in this plot, but we can put an upper limit on the random contribution from the telescope as the standard deviation in the points divided by $\sqrt{2}$ (since the errors in the target filter plus those in R combine in quadrature), which is $\simeq 0.1''$ in all filters.

In order to more carefully determine the telescope contribution to the wavelength dependence of the seeing, we plot the offsets between observation and the $\lambda^{-1/5}$ relation as a function of FWHM as measured in R in Figure 10. Points with offsets from theory greater than $0.3''$, which is significantly larger than the standard deviation of about $0.2''$, are rejected in order to exclude outliers caused by variable atmospheric seeing. Visual inspection of these plots reveal that the telescope's contribution to the wavelength dependence of stellar FWHM has no clear dependence on FWHM, which suggests a constant offset for all cases. The median FWHM_λ – FWHM_R offsets from theory found in this graph ($0.006''$ for $\lambda = U$, $0.055''$ for $\lambda = B$, and -$0.050''$ for $\lambda = V$) provide a measure of the telescope contribution to the FWHM wavelength dependence, which is small and well within the standard deviation

of the observed FWHM's for all images. This telescope contribution, plus the atmospheric contribution given by the $\lambda^{-1/5}$ relation, have been applied to the FWHM in each filter to reduce it to the FWHM that would have been measured in an R-band exposure adjacent in time in Figure 11.

Figure 11 shows a plot of all focus FWHM values in our nine April 1999 – April 2002 observing runs, plus focus FWHM values for eight additional observing runs conducted by one of us (Jansen) for other projects spanning November 2001 – December 2003. All values have been reduced to the R-band using the $\lambda^{-1/5}$ theoretical relation, plus the observational telescope offsets from theory found in Figure 10. The nine April 1999 – April 2002 runs have values that are consistent with the eight November 2001 – December 2003 runs, even though each data set was observed and analyzed independently. The additional runs give us better statistics for more recent years, and thus verify that the observing runs before the telescope improvements (those to the left of the dotted line, which marks the end of the improvements in October 2001) have overall worse stellar FWHM values and larger scatter than those after the telescope improvements. The observing run with the worst individual FWHM measurements was noted to have strong winds from the northeast, which is well-known to cause bad atmospheric seeing conditions at the VATT. Under the best conditions, we were able to measure sub-arcsecond seeing for many of the focus exposures, especially after the telescope improvements in Summer and Fall 2001.

Table 2 summarizes the stellar FWHM's in the galaxy images and the focus exposures. Median stellar FWHM values range from $0.97''$ to $2.15''$ in R focus exposures, and $1.25''$ to $2.40''$ in R galaxy images. The best stellar FWHM measured was $0.65''$ in an R focus exposure, and $0.95''$ in an R galaxy image. This amounts to a linear increase in FWHM of $0.25'' - 0.30''$ in long exposures, which is partially due to vibrations and variable atmospheric seeing, and partially due to the fact that galaxy images may not have been taken at the best telescope focus. Different values may be measured at other telescope sites on Mt. Graham, since there may be a significant telescope contribution to these values, and trees as high as the dome surrounding the VATT site negatively impact the seeing.

5. Conclusions

Figures 1 and 3 and Table 1 suggest that Mt. Graham has a similar average sky brightness as other dark sites, and can occasionally have darker skies than some of the sites reviewed here. We have found that the sky brightness is highly variable with time, both throughout a single observing run and from one run to the next, which is consistent with other findings, as in Krisciunas (1997), who mentions that except for the solar cycle, the most important effect

on sky brightness is random short term variations on timescales of tens of minutes. This makes it difficult to compare sky values from site to site. A more reliable way of comparison would be to amass a large collection of sky surface brightness data over years at each site in order to better understand and remove the short and long term variations in sky brightness, which is currently not fully understood. Various site-dependent factors should also be taken into consideration, such as the linear dependence of sky surface brightness on geomagnetic latitude due to Aurora effects in the Van Allen belt, so that low geomagnetic latitudes have somewhat darker skies than higher latitudes. The direction of pointings towards cities can also affect the sky brightness, with Tuscon and Phoenix city lights slightly increasing the sky brightness at the VATT in that direction by 0.1 mag arcsec^{-2} in U and 0.2 mag arcsec^{-2} in BVR. However, measurements made toward the nearest city, Safford, are not measurably brighter than other directions (thanks to dark sky ordinances in Safford and shielding from the mountain peak at the VATT site). Nightly trends are also seen, with sky brightness values decreasing throughout at least the first half of the night by an amount that depends, at least, on the elevation of the observing site. Mt. Graham's high elevation contributes in this and many other ways to darker night skies, and the minimal effect of city lights at this location make Mt. Graham a prime dark-sky site that can easily compete with other dark sites around the world.

The FWHM of stars in images we took at the VATT have improved considerably (by 0.45″) since maintenance operations for the Summer and Fall of 2001 corrected secondary mirror vibrations and improved the telescope pointing map. Figures 7, 8 and 11, and Table 2 show our stellar FWHM results. We were able to get sub-arcsecond seeing on occasion, especially in short (several second) focus exposures, which are less affected than long object exposures by vibrations, variable atmospheric seeing, and slipping of the telescope out of focus as the temperature changes. Because of this, the FWHM values given by focus exposures are closer to the true atmospheric seeing (by about 0.3″) than those from faint object images.

It should also be noted that there may be a significant telescope contribution to the seeing measured at the VATT, and that the atmospheric seeing may be different at other likely locations on Mt. Graham since the presence of trees as tall as the dome around the VATT have a negative impact on the seeing at that telescope. Good seeing is not crucial to our purposes of performing surface photometry on extended galaxies, but observers who desire smaller point spread functions (PSF's) should be able to improve on our numbers by focusing more often (at least once an hour, and more often at the beginning of the night when the temperature is more unstable), and refocusing for each individual filter rather than using the focus of one filter for all filters. It should also be noted that the seeing is highly dependent on the weather, with strong northeasterly winds contributing to much

worse seeing.

VAT was supported in part by the NASA Space Grant Graduate Fellowship at ASU and in part by NASA grant GO-9824.1 and GO-9124.1. RAJ acknowledges partial support from NASA grant GO-9892.1. We wish to thank the staff at the VATT, especially Richard Boyle, Matthew Nelson, and Christopher Corbally for their gracious help and support. We also wish to thank our many co-observers: Claudia Chiarenza, Thomas McGrath, Luis Echevarria, Hu Zhan, Seth Cohen, Stephen Odewahn, Richard de Grijs, Corey Bartley, Joe Baker, Jason Mager, and Kazuyuki Tamura. RAJ wishes to extend particular thanks to Elizabeth Barton, who was PI on several of the programs for which FWHM measurements are presented in this paper. We also thank the referee, Wes Lockwood, who offered very knowledgeable and helpful comments. On behalf of all MGIO observers, we wish to thank the Tucson and Safford city councils for passing strict low pressure sodium light ordinances, which make a noticeable difference in the sky brightness at Mt. Graham.

REFERENCES

Benn, C.R., and Ellison, S.L. 1998, NewAR, 42, 503

Bertin, E., and Arnouts, S. 1996, AJ, 117,393

Coulman, C.E. 1985, ARA&A, 23, 19

Fried, D.L. 1965, OSAJ, 55, 1427

Garstang, R.H. 1989, PASP, 101, 306

Kolmogorov, A.N. 1941, in Tikhomirov, V.M., ed, Selected works of A.N. Komogorov, Mathematics and its applications (Soviet series), Klewer Academic press (1991)

Krisciunas, K., and Schaefer, B. 1991, PASP, 103, 1033

Krisciunas, K. 1997, PASP, 109, 1181

Landolt, A.U. 1992, AJ, 104, 340

Massey, P., and Foltz, C.B. 2000, PASP, 112, 566

Odewahn, S.C., Cohen, S.H., Windhorst, R.A., Philip, N.S. 2002, 568, 539

Patat, F. 2003, A&A, 400, 1183

Roddier, F. 1981, in Wolf E., ed, Progress in Optics 19, North Holland Publ., Amsterdam

Tatarski, V.I. 1961, Wavefront Propagation in a Turbulent Medium, Dover, New York

Walker, A. 1987, NOAO Newsletter, No. 10, 16

Walker, M. 1988, PASP, 100, 496

Fig. 1.— Sky surface brightness in stacked galaxy images taken at the VATT between April 1999 and April 2002 in U, B, V and R. Each of our observing runs is indicated in a separate sub-panel. Measurements obtained under non-photometric conditions are represented by open circles, while measurements from photometric nights (zeropoint variations $\lesssim 3\%$ throughout the night) are indicated by asterisks. Within a given run, the sky is brighter during non-photometric than photometric conditions. The sky surface brightness can be highly variable on monthly, nightly, and tens of minutes time scales. Dotted lines represent the average values at Mt. Hopkins/Kitt Peak (converted to broad-band from spectrophotometry) over four nights in 1998 and 1999 (Massey & Foltz 2000), just before solar maximum (2000–2001).

Fig. 2.— The dependence of the sky surface brightness, normalized to the median sky surface brightness for that observing run, on angular distance from the Moon for different Moon illuminations. Open symbols represent data that were taken during non-photometric nights, solid ones represent data taken during photometric nights. Points are coded according to filter of observation as indicated in the upper left panel. A clear dependence on angular distance to the Moon is only seen for illumination $\gtrsim 20\%$. Straight lines represent linear least-squares fits to the data in each passband for data with $\sec z < 2$. The dependence on Moon distance is stronger at shorter wavelengths. In general, our galaxy images were taken well away from the Moon and mostly during dark nights ($\lesssim 4$ days from New Moon), and thus the average sky surface brightness values presented in this paper are not strongly affected by the Moon.

Fig. 3.— Median sky surface brightness of all photometric stacked galaxy images taken at the VATT with airmass ($\sec z$) < 1.2, rejecting no more than one obvious outlier per data point. Error bars represent the 25% – 75% quartile range. The horizontal lines represent the average sky surface brightness near zenith at Mt. Hopkins and Kitt Peak, Arizona (Massey & Foltz 2000; converted from spectrophotometry) [*dotted*], at Cerro Tololo, Chile (Walker 1987, and 1987–1988 results at *http* : *//www.ctio.noao.edu/site/pachon_sky/*) [*dashed*] and at La Palma, Canary Islands, Spain (Benn & Ellison 1998) [*dot-dashed*]. A comparison with other sites is given in Table 1.

Fig. 4.— Sky brightness normalized to the median sky for the observing run, where $\sec z \leq 1.3$ and moon illumination $\leq 20°$. Non-photometric points (open circles for $20° \leq z < 40°$, and asterisks for $z \geq 40°$) are arbitrarily offset from photometric points (solid circles for $20° \leq z < 40°$, and triangles for $z \geq 40°$). The normalized median is marked with a dotted (non-photometric) or dashed (photometric) horizontal line. Vertical dotted lines mark the general direction of three cities that may affect the sky brightness.

Fig. 5.— Sky brightness normalized to the median sky for the observing run, where $\sec z \leq 1.3$ and moon illumination $\leq 20°$. Non-photometric points (open circles) are arbitrarily offset from photometric points (solid circles). The normalized median is marked with a dotted (non-photometric) or dashed (photometric) line. The beginning and end of the night is defined by the end and beginning of astronomical twilight for the mid-point of the observing run, such that dusk is at fraction=0, and dawn at fraction=1. Solid lines are the linear least-squares fit to the data, excluding measurements taken within 0.5 hours of twilight.

Fig. 6.— Object FWHM versus apparent magnitude in a single galaxy field. We use the fact that the FWHM of a star does not depend on its brightness to separate stars and extended objects, as labeled on the plot. For the purpose of our semi-automated seeing measurements, we excluded saturated stars and stars that are too faint to yield reliable measurements. The solid box encloses the objects that were used to compute the mean stellar FWHM for this field (*dotted horizontal line*).

Fig. 7.— Median stellar FWHM in images taken at the VATT between April 1999 and April 2002 in U,

B, V and R. Each of our observing runs is indicated in a separate sub-panel. Measurements obtained under non-photometric conditions are represented by open circles, while measurements from photometric nights (zeropoint variations $\lesssim 3\%$ throughout the night) are indicated by asterisks. The solid squares represent the stellar FWHM corresponding to the best focus setting as measured in short focus exposures. These tend to be smaller than or equal to the FWHM's measured in adjacent object exposures. We typically focused the telescope in U, since that is where most of our galaxy images would be taken.

Fig. 8.— Historical trend in our FWHM measurements. **Solid circles:** Median stellar FWHM at low airmass ($\sec z < 1.2$) measured in our stacked galaxy images. **Open circles:** Median FWHM of the best focus setting measured in short focus exposures. Error bars represent the 25% – 75% quartile range for each run. Improvements to the telescope in Summer and Fall 2001 significantly reduced the stellar FWHM's measured during the later runs.

Fig. 9.— **Open circles:** stellar FWHM of each stacked galaxy image minus the stellar FWHM in the R-band image of that galaxy, producing a measure of the FWHM offset between filters at the VATT. Outliers are due to highly variable seeing conditions or cases where a focus exposure was taken in between observations for a single galaxy. Galaxies where observations in each filter were not carried out immediately after one another are not included on this plot. **Crosses:** the median FWHM_λ – FWHM_R offset from theory for each filter. The boxes surrounding the medians enclose the 25% – 75% quartile range. **Solid line:** The value offsets would have if the FWHM's followed the theoretical $\lambda^{-1/5}$ dependence, using the median FWHM_R value of $1.63''$. The divergence of theory from the median observed offsets are due to specific telescope properties at the VATT that cause a systematic contribution from the telescope to the wavelength dependence of the seeing. The scatter in this plot gives random offsets from theory which are partially due to atmospheric variations, and partly due to telescope vibrations (which is particularly important for the earlier runs). This vibrational component cannot be separated from the atmospheric effects, but it cannot be larger than the standard deviation of the points, which is $\simeq 0.2''$ in all filters.

Fig. 10.— Comparison of the theoretical $\lambda^{-1/5}$ wavelength dependence of stellar FWHM to the observed wavelength dependence for each image, for the purpose of reducing FWHM values to the R-band in order to inter-compare focus exposures taken in different filters (as in Figure 11). We find the observed FWHM in each passband (UBV) minus the FWHM in the reference filter, R, and subtract this from the theoretical result, then plot this offset versus the observed FWHM in R. Galaxies where observations in each filter were not carried out immediately after one another are not included. Points with offsets from theory greater than $0.3''$ (which is outside the standard deviation of $0.2''$ for all of the points) were rejected to avoid outliers caused by variable atmospheric conditions. There is no strong dependence on FWHM_R for this offset in any filter, and thus we apply a constant small telescope correction to all FWHM values in Figure 11 of the median (observation-theory) offset in UBV (listed in the figure and marked by dotted lines), plus the atmospheric contribution given by the $\lambda^{-1/5}$ relation.

Fig. 11.— VATT focus exposure stellar FWHM values normalized to the R-band using the theoretical atmospheric $\lambda^{-1/5}$ dependence plus the observational median telescope contribution offsets found in Figure 10. This plot includes observing runs carried out by one of us (R. Jansen), in addition to the observing runs the rest of this paper focuses on. The worst FWHM values were measured when strong winds were blowing from the Northeast, which always results in particularly bad seeing conditions at the VATT. Sub-arcsecond R-band seeing was reached on occasion throughout this time period. FWHM values are highly variable, although an overall improvement in median FWHM and scatter is apparent in the observing runs

following telescope improvements made in Summer and Fall 2001. The dotted line marks the end of the implementation of these improvements.

Table 1. Average Photometric Sky Surface Brightness (μ) Near Zenith at Various Sites.

Site	Condition	Obs. Dates	μ_U	μ_B	μ_V	μ_R
Mt. Graham[1]	Darkest run	U: 02/00, BVR: 02/01	22.38	22.86	21.72	21.19
Mt. Graham[1]	All runs	04/99–04/02	22.00	22.53	21.49	20.88
Mt. Graham[1]	Brightest run	04/99	21.68	22.01	21.04	20.46
Mt. Hopkins[2]	···	11/98	···	22.63	21.46	···
Kitt Peak[2]	···	11/99	···	22.63	21.44	···
Mauna Kea[3]	Solar min.	96	···	22.84	21.91	···
Mauna Kea[3]	Solar max.	92	···	22.22	21.29	···
La Palma[4]	···	87-96	22.0	22.7	21.9	21.0
ESO/La Silla[5]	···	04/00–09/01	22.3	22.6	21.6	20.9
Cerro Tololo[6]	···	87–88	22.0	22.7	21.8	20.9
Cerro Tololo[7]	···	97	···	22.8	22.2	···

Note. — All sky surface brightness values have units of mag arcsec^{-2}.

[1]Mean error on mean Mt. Graham values $\lesssim 0.04$ mag arcsec^{-2}.

[2]Massey & Foltz 2000. Calculated from spectrophotometry.

[3]Krisciunas 1997.

[4]Benn & Ellison 1998. Solar min., high galactic and ecliptic latitude. Measured 0.4 mag arcsec^{-2} brighter at solar max.

[5]Patat 2003. Values corrected to zenith.

[6]Walker 1987, and 1987–1988 results at *http* : *//www.ctio.noao.edu/site/pachon_sky/*

[7]Phillips 1997 results at *http* : *//www.ctio.noao.edu/site/pachon_sky/*

Table 2. Median stellar FWHM measurements at the VATT.

type	date	U-band	B-band	V-band	R-band
Best median focus[1]	2/01 & 10/02	···	···	···	$0.97'' \pm 0.06''$
Worst median focus[1]	4/01	···	···	···	$2.15'' \pm 0.42''$
Best FWHM in single focus exposure[1]	2/01	···	···	···	$0.65''$
All galaxy images[2]	4/99–2/01	$2.01'' \pm 0.25''$	$2.01'' \pm 0.34''$	$1.86'' \pm 0.39''$	$1.81'' \pm 0.24''$
All galaxy images[3]	5/01–4/02	$1.57'' \pm 0.10''$	$1.56'' \pm 0.12''$	$1.41'' \pm 0.12''$	$1.36'' \pm 0.08''$
Best median in galaxy images[4]	4/02	$1.36'' \pm 0.03''$	$1.42'' \pm 0.06''$	$1.23'' \pm 0.04''$	$1.25'' \pm 0.05''$
Worst median in galaxy images[4]	4/01	$2.66'' \pm 0.12''$	$2.65'' \pm 0.22''$	$2.67'' \pm 0.26''$	$2.40'' \pm 0.11''$
Best FWHM in single galaxy image	UBV: 2/01, VR: 4/02	$1.12''$	$1.12''$	$1.03''$	$0.95''$

Note. — Stellar FWHM values measured in focus frames are closer to the true atmospheric seeing than stellar FWHM values measured in galaxy images, because focus exposures are short (a few seconds compared to a few minutes) and record the best telescope focus (which may have deteriorated in galaxy exposures). Focusing must be done frequently (at least once an hour, possibly more at the beginning of the night and less toward the end of the night) in order to obtain the best stellar FWHM values in deep object exposures. For our galaxy images we typically focused in U. Focusing in each filter separately would result in smaller stellar FWHM's in the other pass-bands.

[1]Exposures taken in filters other than R were reduced to R using the theoretical $\lambda^{-1/5}$ dependence and the observed contribution from the telescope added in quadrature. Median values are per observing run.

[2]Before telescope improvements in Summer and Fall 2001.

[3]After telescope improvements in Summer and Fall 2001.

[4]Median values are per observing run.

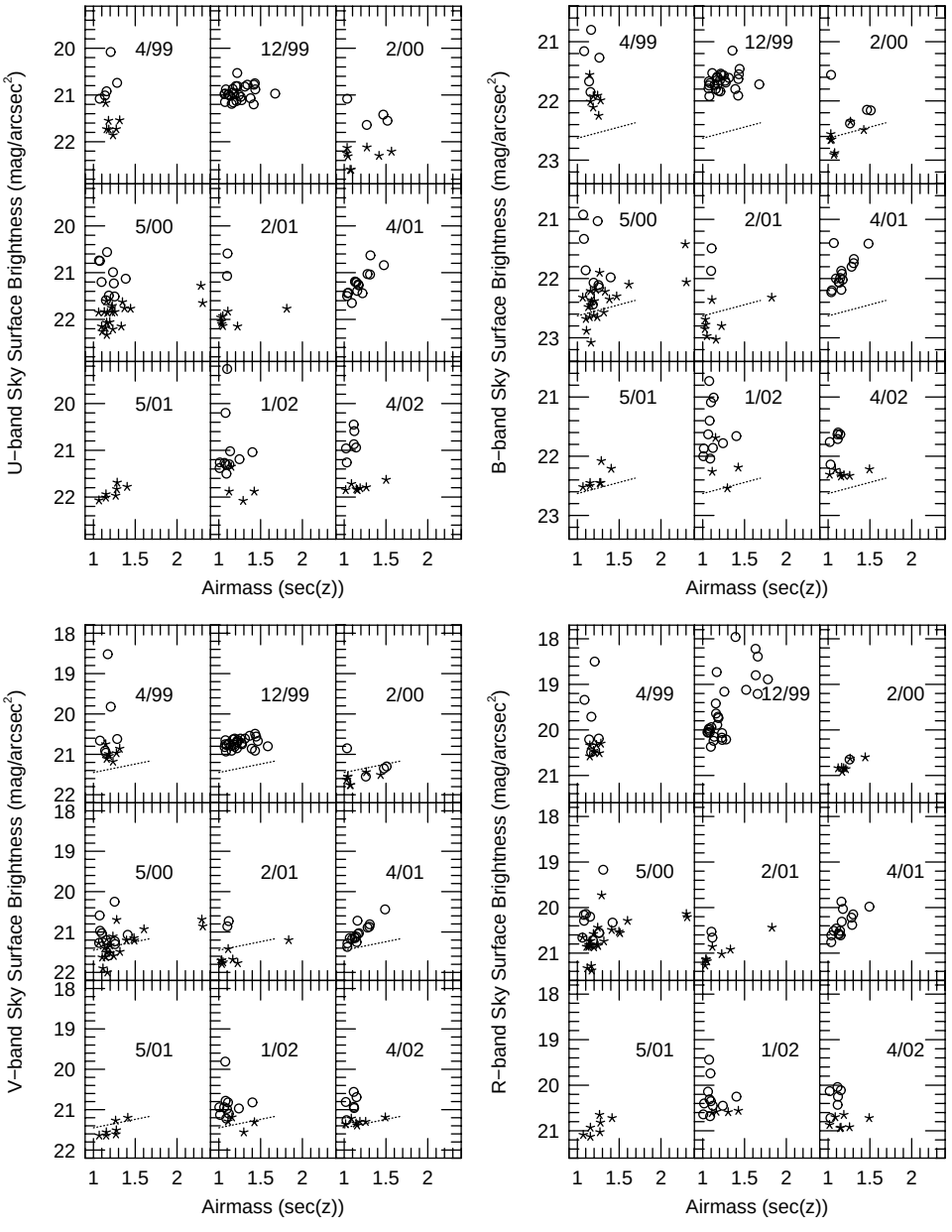
U−band Sky Surface Brightness (mag/arcsec^2)
B−band Sky Surface Brightness (mag/arcsec^2)
V−band Sky Surface Brightness (mag/arcsec^2)
R−band Sky Surface Brightness (mag/arcsec^2)
4/99
12/99
2/00
5/00
2/01
4/01
5/01
1/02
4/02
Airmass (sec(z))

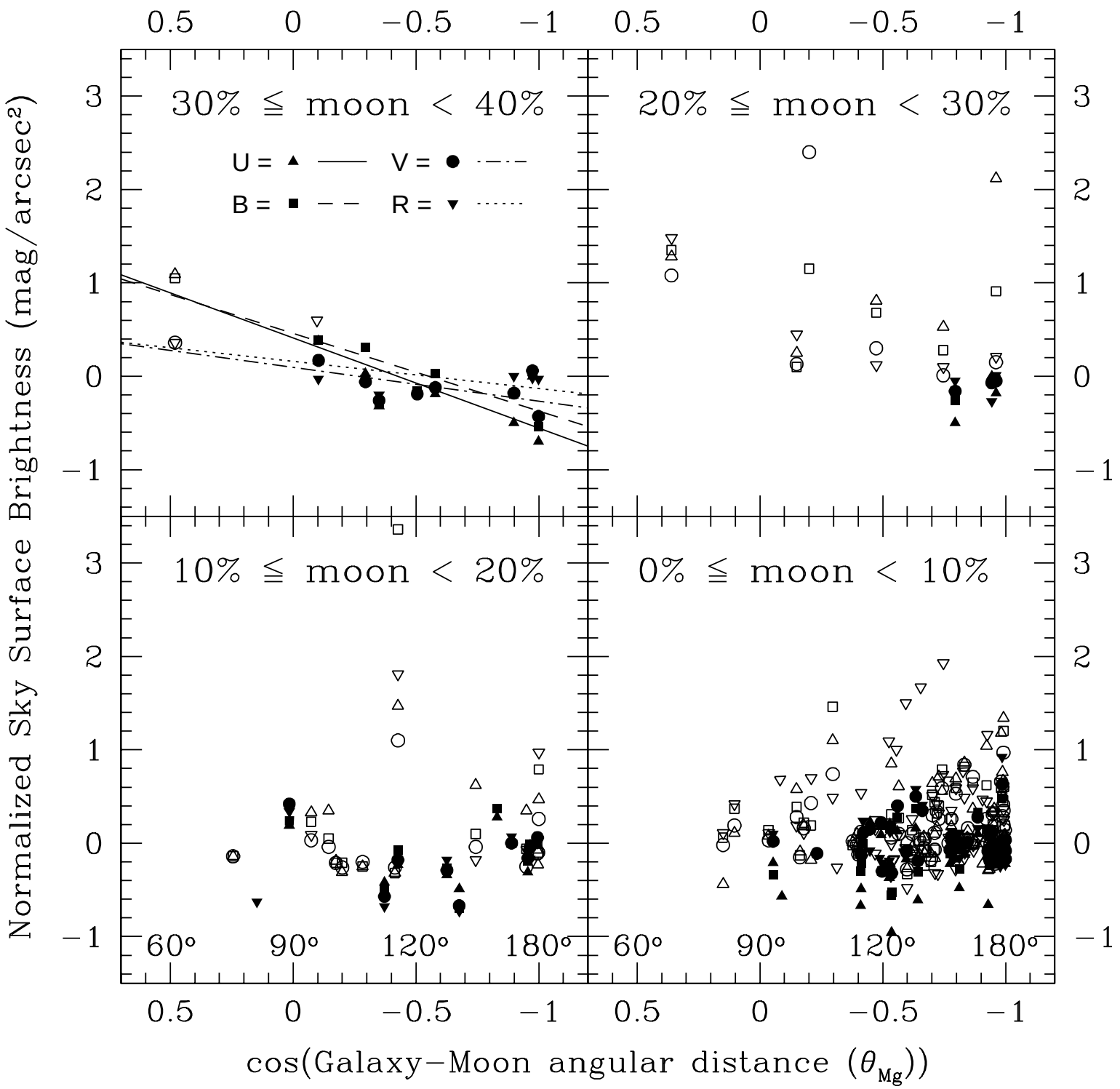
30% ≦ moon < 40%
20% ≦ moon < 30%
10% ≦ moon < 20%
0% ≦ moon < 10%
U = ▲ —— V = ● -·-·-
B = ■ – – R = ▼ ·····
Normalized Sky Surface Brightness (mag/arcsec²)
cos(Galaxy−Moon angular distance (θMg))
0.5
0
−0.5
−1
3
2
1
0
−1
60°
90°
120°
180°

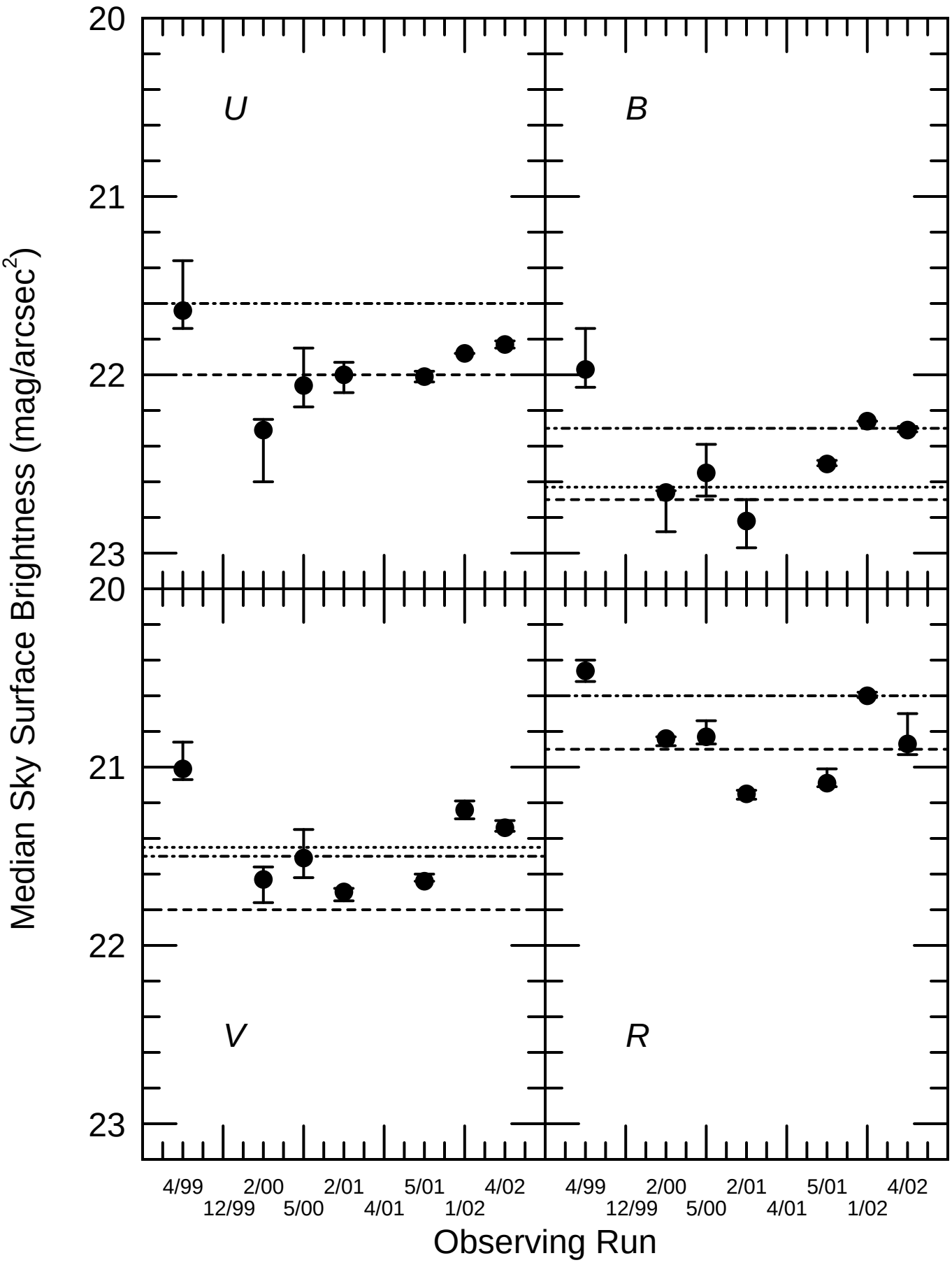
U
B
V
R
20
21
22
23
Median Sky Surface Brightness (mag/arcsec^2)
4/99
12/99
2/00
5/00
2/01
4/01
5/01
1/02
4/02
Observing Run

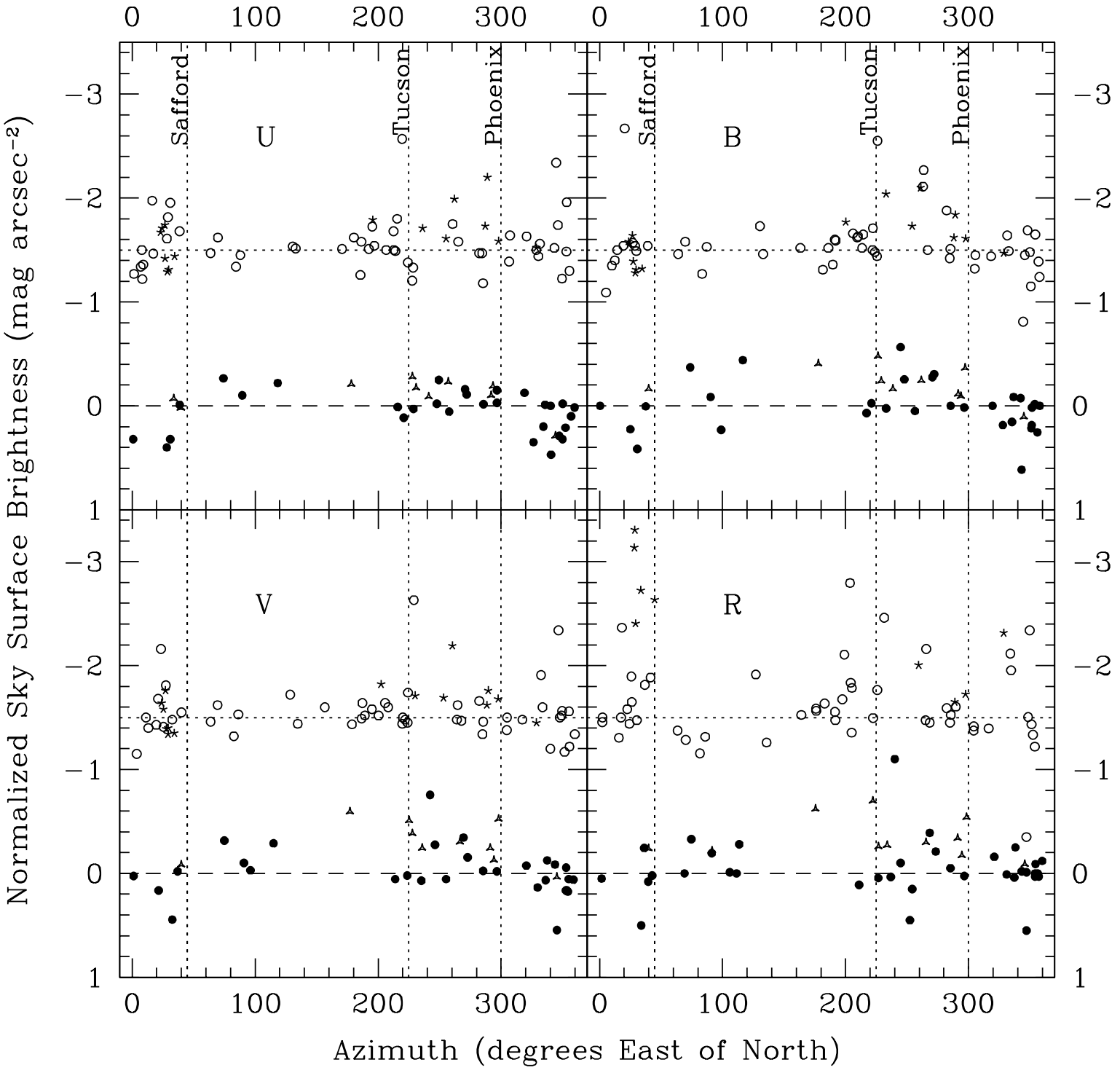
U
B
V
R
Safford
Tucson
Phoenix
0
100
200
300
−3
−2
−1
0
1
Normalized Sky Surface Brightness (mag arcsec⁻²)
Azimuth (degrees East of North)

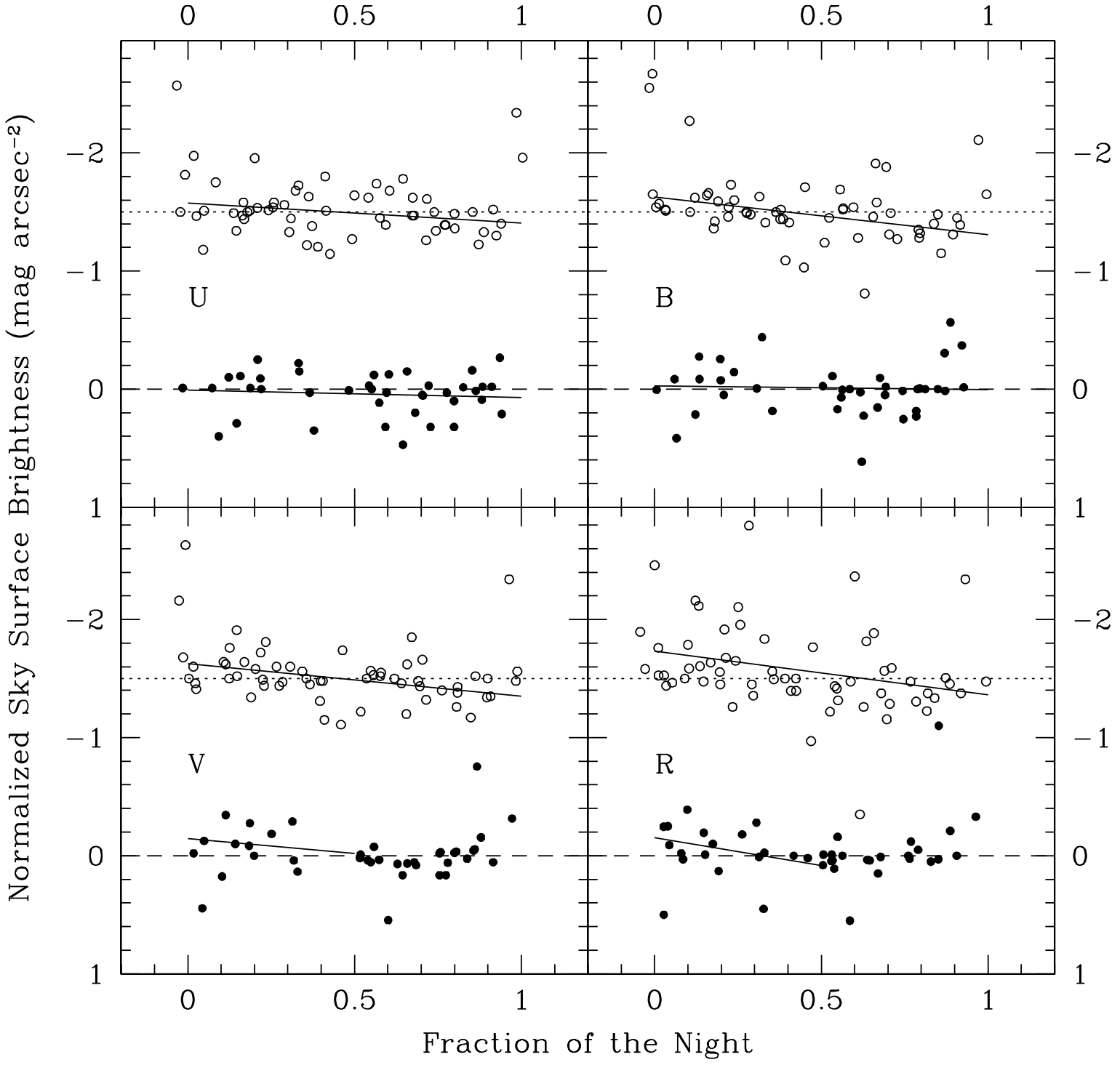
Normalized Sky Surface Brightness (mag arcsec⁻²)
Fraction of the Night
U
B
V
R
0
0.5
1
−2
−1
0
1

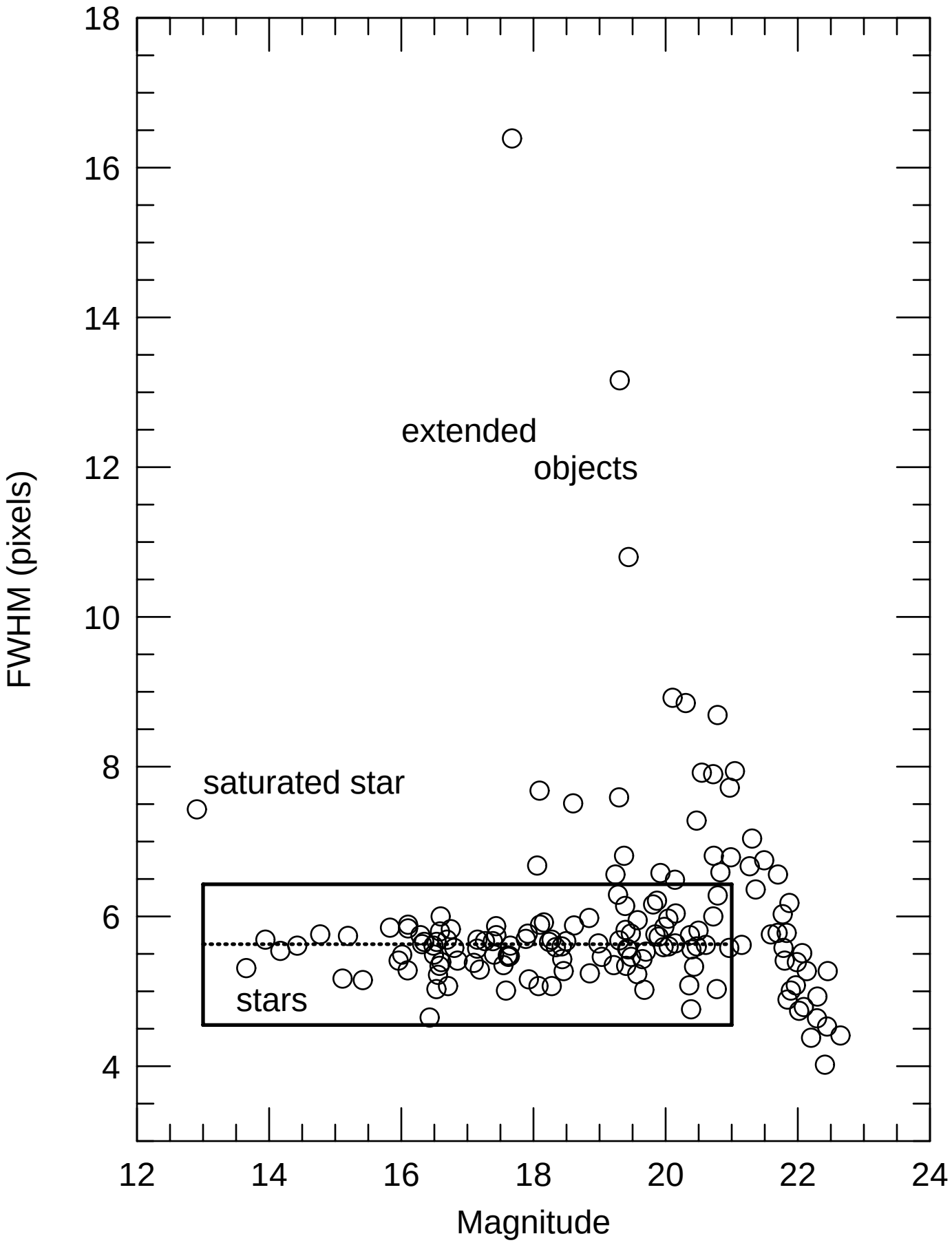
18
16
14
12
10
8
6
4
FWHM (pixels)
extended
objects
saturated star
stars
12
14
16
18
20
22
24
Magnitude

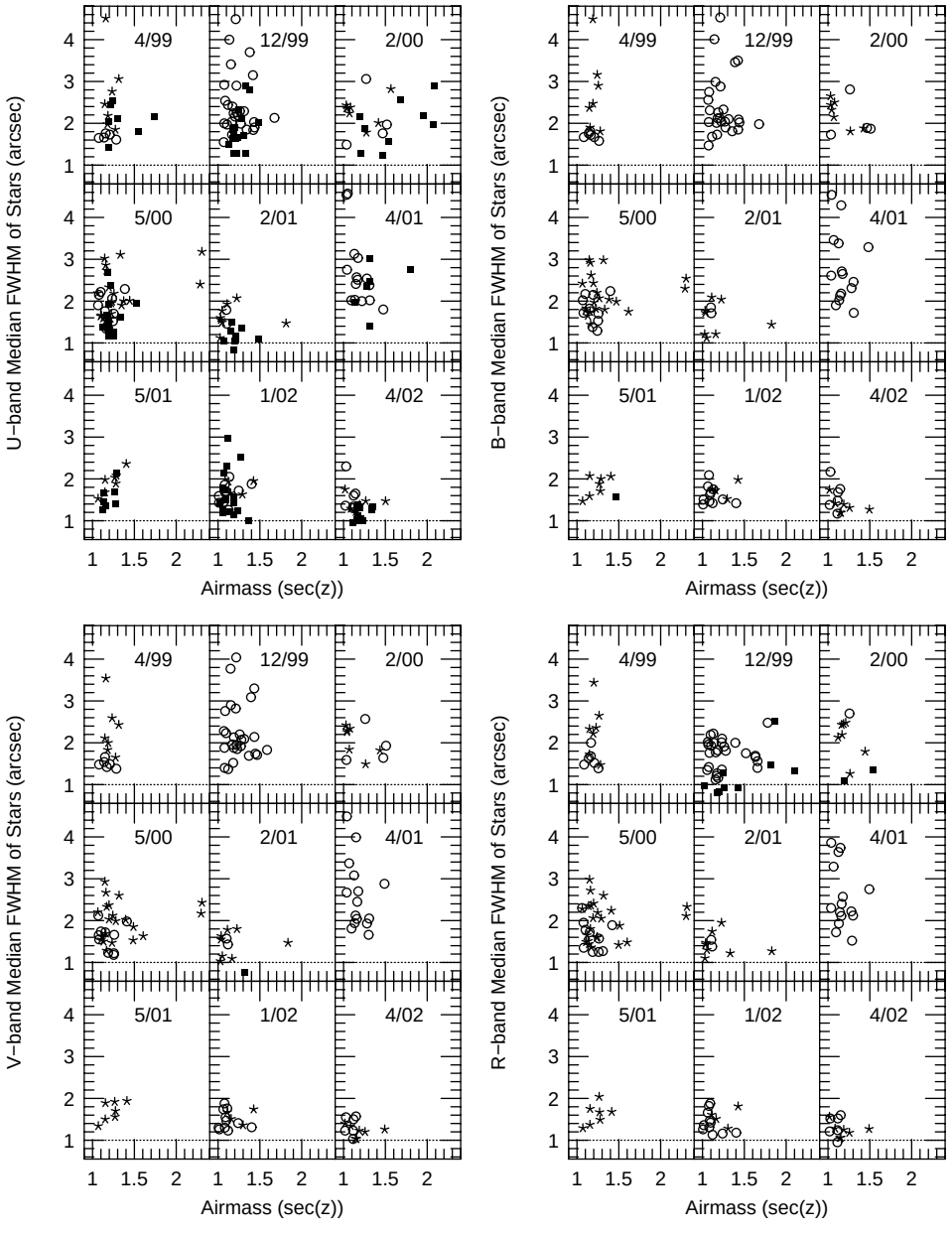
U−band Median FWHM of Stars (arcsec)
B−band Median FWHM of Stars (arcsec)
V−band Median FWHM of Stars (arcsec)
R−band Median FWHM of Stars (arcsec)
4/99
12/99
2/00
5/00
2/01
4/01
5/01
1/02
4/02
Airmass (sec(z))

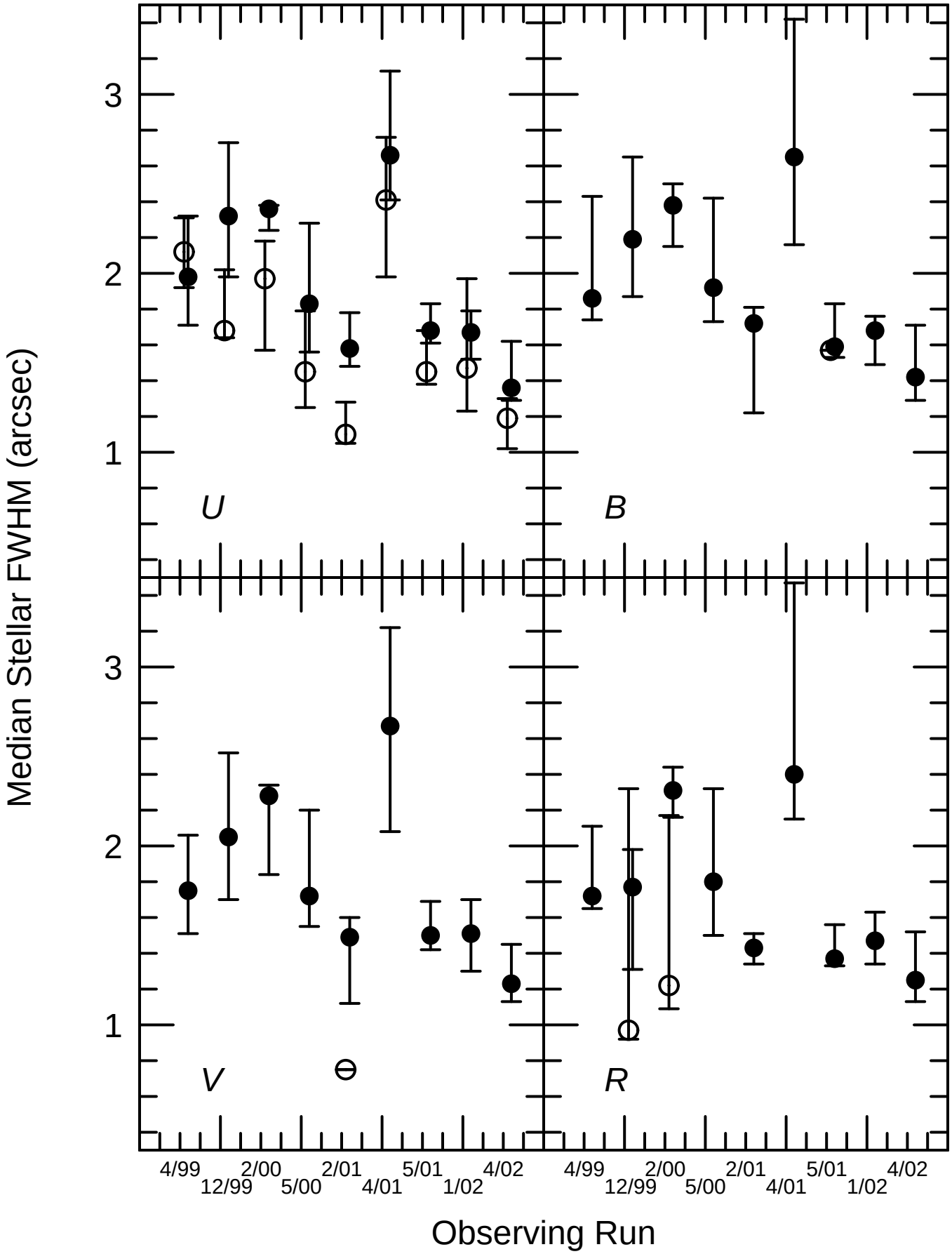
Median Stellar FWHM (arcsec)
3
2
1
U
B
V
R
4/99
12/99
2/00
5/00
2/01
4/01
5/01
1/02
4/02
Observing Run

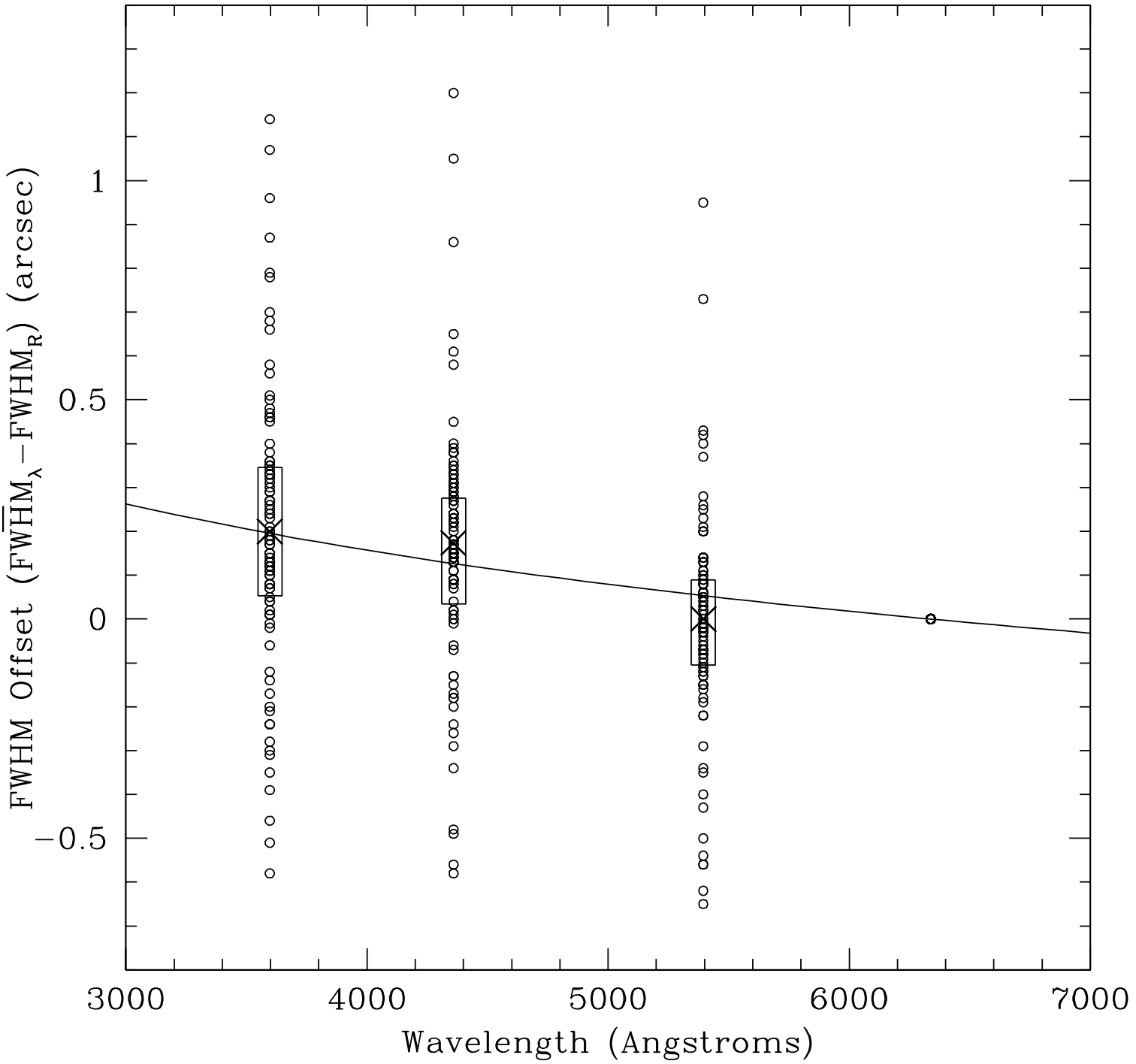
FWHM Offset ($\overline{FWHM}_\lambda - FWHM_R$) (arcsec)
1
0.5
0
−0.5
3000
4000
5000
6000
7000
Wavelength (Angstroms)

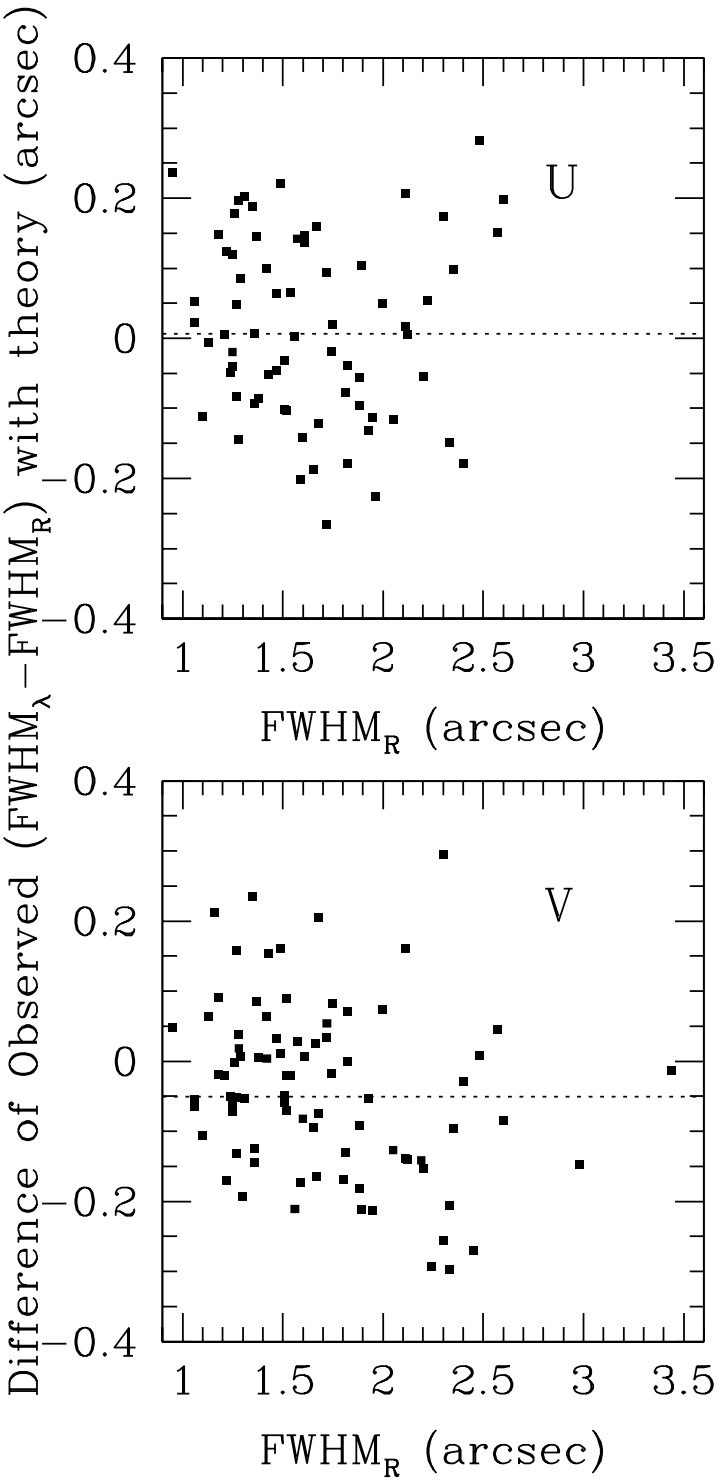

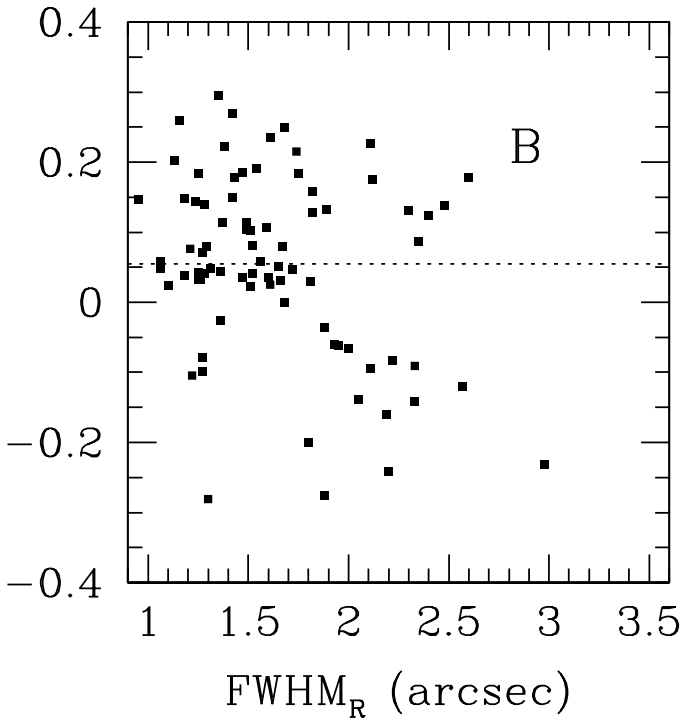

Median telescope contribution

to wavelength dependence of seeing:

$\mathrm{FWHM_U} - \mathrm{FWHM_R} = +0.006''$

$\mathrm{FWHM_B} - \mathrm{FWHM_R} = +0.055''$

$\mathrm{FWHM_V} - \mathrm{FWHM_R} = -0.050''$

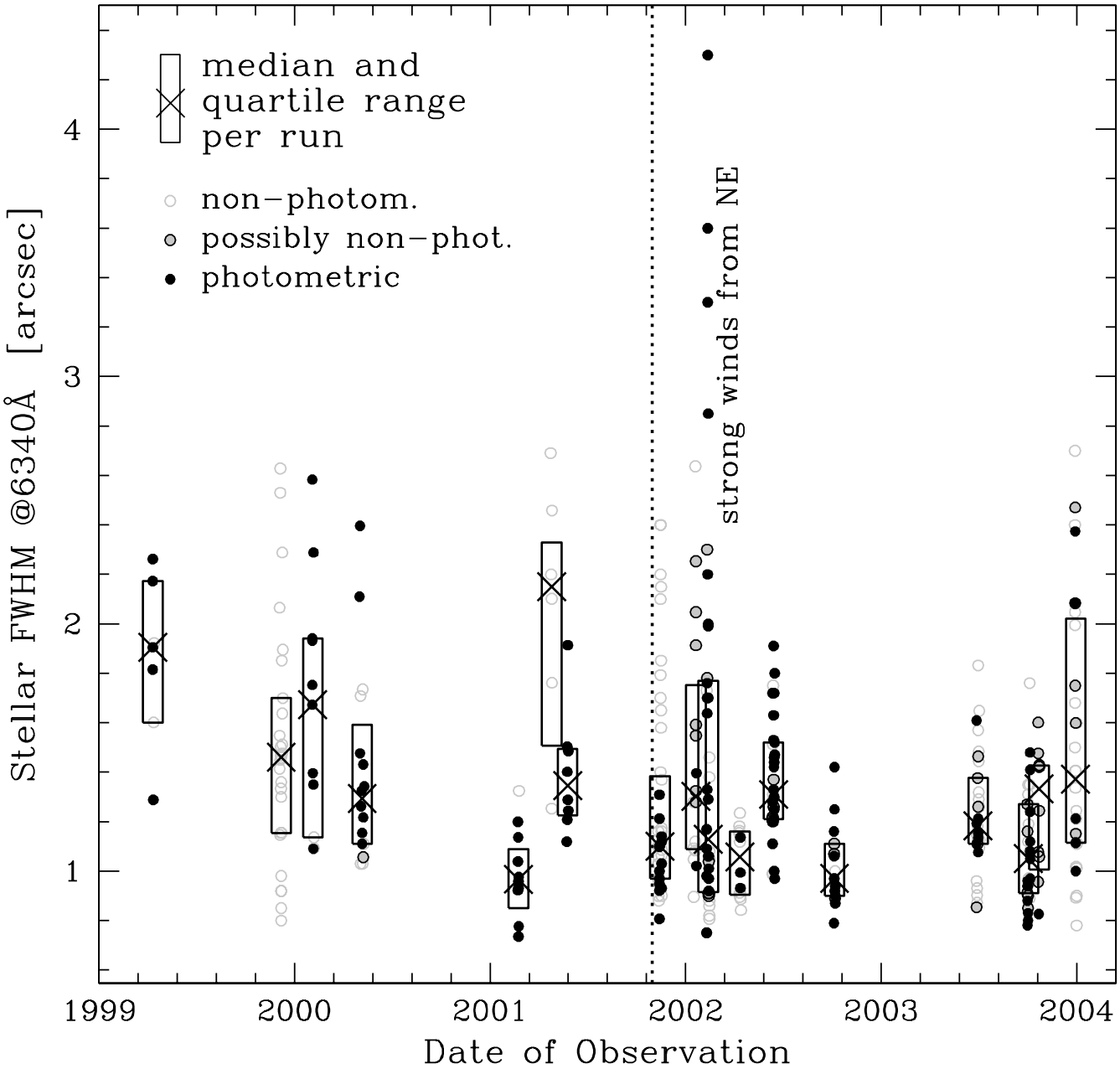
median and
quartile range
per run
non−photom.
possibly non−phot.
photometric
strong winds from NE
Stellar FWHM @6340Å [arcsec]
1
2
3
4
1999
2000
2001
2002
2003
2004
Date of Observation